CrystEngComm

Accepted Manuscript

ROYAL SOCIETY OF CHEMISTRY

www.rsc.org/crystengcomm

Cite this: DOI: 10.1039/c0xx00000x

www.rsc.org/xxxxxx

ARTICLE TYPE

Full-capped 12-S-atom TTP derivatives (BV-TTP, BE-TTP, EM-TTP and EV-TTP): Syntheses, structures and charge transport properties†

Qi Fang,*[ab] Hong-feng Chen,[a] Hong Lei,[c] Gang Xue[a] and Xia Chen[a]

Received (in XXX, XXX) Xth XXXXXXXXX 20XX, Accepted Xth XXXXXXXXX 20XX

DOI: 10.1039/b000000x

By π-extending and ring-capping the bis-fused TTF moiety (namely TTP), several electrically conductive crystals of 12-S-atom TTP derivatives have been synthesized: (1) bis(vinylenedithio)-TTP which can be isolated as triclinic $P\bar{1}$ (***t*-BV-TTP**) and monoclinic $P2_1$ (***m*-BV-TTP**) polymorphs separately, (2) bis(ethylenedithio)-TTP (**BE-TTP**), (3) ethylenedithio-methylenedithio-TTP (**EM-TTP**), (4) ethylenedithio-vinylenedithio-TTP (**EV-TTP**). The structures of ***t*-BV-TTP** and **EM-TTP** crystals can be classified as all-parallel *β*-type, in which all molecules in the same 2-D molecular slab or in different slabs are all parallel packed. Differently, ***m*-BV-TTP** and **BE-TTP** crystals can be described as herring-bone *β*-type, in which the molecules in neighboring 2-D slabs are alternately in two directions. Among the above four *β*-type structures, **EM-TTP** crystal shows the highest conductivity ($\sigma = 7\times10^{-3}\ \Omega^{-1}cm^{-1}$ along [100] direction). The **EV-TTP** crystal belongs to a kind of three-by-three *κ*-type structure and its conductivity was measured to be $3\times10^{-3}\ \Omega^{-1}cm^{-1}$ along [100] direction. The calculated hole mobilities of the title TTP derivatives, by DFT method and the host-caged approach, are larger than that of the dithiophene-TTF (DT-TTF) crystal.

1 Introduction

The sulfur-rich π-donor tetrathiafulvalene (TTF) is a pioneer and evergreen compound in organic electronics which has stimulated intense and steady interest for more than 40 years.[1] Among the numerous TTF derivatives, bis(ethylenedithio) tetrathiafulvalene (BEDT-TTF or BE-TTF in short) stood out for its large number of superconductive $(BE\text{-}TTF)_2X$ radical-cation salts.[2] In 1993, bis-fused TTF, namely 2,5-bis(1,3-dithiol-2-ylidene)-1,3,4,6-tetrathiapentalene (BDT-TTP or TTP in short), as another promising TTF derivative was reported,[3] and series of TTP-based conducting radical-cation salts followed.[4] Soon afterwards, the 12-S-atom TTP derivative 2,5-bis(4,5-ethylenedithio-1,3-dithiol-2-ylidene)-1,3,4,6-tetrathiapentalene (**BE-TTP**, see Scheme 1), which combines the structural ingredients of BE-TTF and TTP to have a larger π-dimension, was reported and its radical-cation salt $(BE\text{-}TTP)_2I_3$ exhibited high conductivity.[5,6] The X-ray structure of $(BE\text{-}TTP)_2I_3$ was reported at the level of $R_1 = 0.174$,[5] while there was no structure report about the neutral **BE-TTP** crystal because of its poor solubility in solvents and the difficulty in crystal growth. EP-TTP, together with its conducting radical salt $(EP\text{-}TTP)_2Au(CN)_2$, is another known full-capped 12-S-atom TTP derivative, in which one end is capped by $-CH_2CH_2-$ group and the other end by $-CH_2CH_2CH_2-$ group.[7] The practice of synthesizing a number of "half-capped" TTP derivatives (see Scheme 1) reflected the trade-off between solubility and conductivity.[8] The non-capped TTM-TTP (see Scheme 1), in which the TTP core is symmetrically attached by four methylthio groups, was reported early in 1992.[9] Since then more than ten TTM-TTP based structures (most of which are conducting radical-cation salts) have been reported.[10] The non-capped TTP derivatives are relatively easy to synthesize due to their relatively large solubility. However, as Mori pointed out, the terminal methylthio groups are harmful to two-dimensional network of the donors.[10a]

It was believed for a long time that an organic conductor should consist of two components to form donor-acceptor complex or radical-counterion salt. To our knowledge, the first remarkable single-component organic conductor is the TTF derivative BTQBT (see Scheme 1), which was reported in 1992 with a conductivity of $8\times10^{-4}\ \Omega^{-1}cm^{-1}$.[11] One merit of the single-component organic conductive crystals is that they are available to fabricate semi-conductor devices such as organic field-effect transistors (OFETs) by vapour deposition and solution-based methods. The conductivity of the organic crystals of TTF and TTP derivatives can be increased by two or more orders of magnitude when the molecular π-dimension is extended from 8-S-atom to 12-S-atom.[12,13] The crystal of the non-capped TTC_4-TTP (see Scheme 1), in which the TTP core is attached by four *n*-butylthio chains, exhibited a conductivity of $2\times10^{-4}\ \Omega^{-1}cm^{-1}$.[12] When the π-dimension is extended to 16-S-atom such as TTC_3-TTPY, in which the tris-fused TTF core (namely TTPY) is attached by four propylthio chains, the conductivity of a crystal was measured to be $1\times10^{-3}\ \Omega^{-1}cm^{-1}$ by the two-probe method.[13] If the terminal pair of flexible alkylthio chains in the above examples were replaced by a rigid "capped" moiety such as $-SCH_2S-$ group to benefit the molecular packing, we believe that the conductivity should be considerably increased.

We have recently developed a method (see experimental section) to deal with the solubility problem and synthesized several full-capped 12-S-atom TTP derivatives (symmetric **BV-TTP** and **BE-TTP**, and non-symmetric **EM-TTP** and **EV-TTP**, see Scheme 2). These TTP derivatives exhibit remarkable conductivities (see Table 2). The details will be reported below.

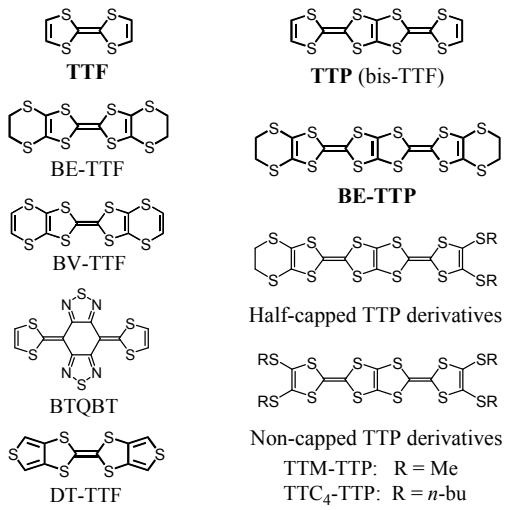

Scheme 1 Several TTF and TTP derivatives

2 Results and discussion

2.1 Syntheses and redox properties

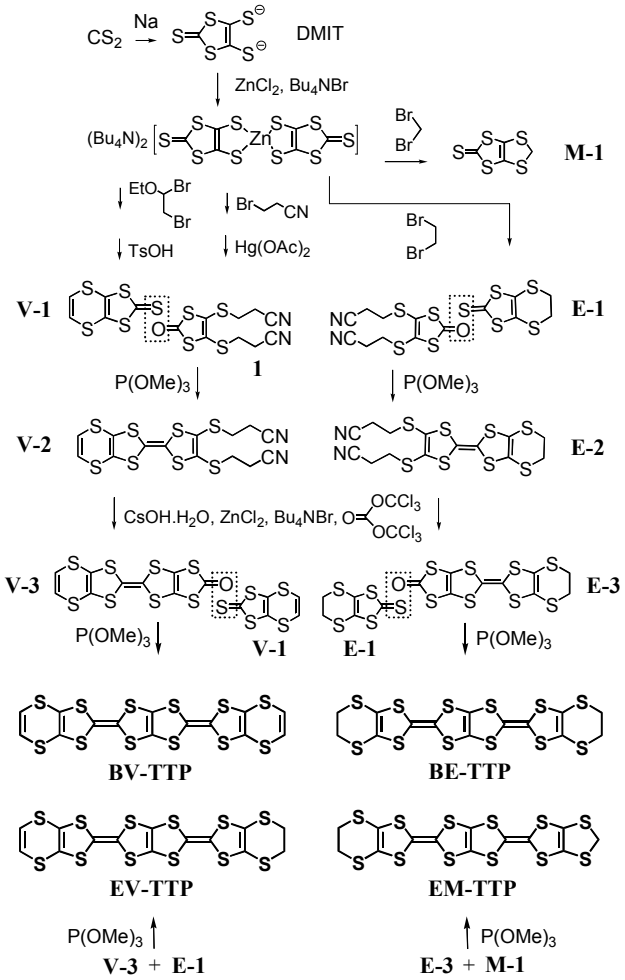

Scheme 2 Syntheses of the title TTP derivatives

As shown in Scheme 2, the syntheses began with CS_2, which reacted with Na in the presence of DMF. [14] The resultant DMIT dianion is unstable but can form stable complexes such as $(Bu_4N)_2[Zn(dmit)_2]$ or neutral species such as compound **1**.[14,15] The primary precursor **E-1** or **M-1** were obtained by end-capping DMIT with $-CH_2CH_2-$ or $-CH_2-$ group *via* the nucleophilic attack of $(Bu_4N)_2[Zn(dmit)_2]$ on $BrCH_2CH_2Br$ or CH_2Br_2, while the **V-1** needs an additional step to afford the terminal double bond.[16] By cross-coupling equimolar amounts of **V-1** (or **E-1**) and compound **1** in hot $P(OMe)_3$, the secondary precursor **V-2** (or **E-2**) was produced with moderate yield (27% for **V-2** and 59% for **E-2**) due to the by-products of the **1** self-coupling (20~30%) and the **V-1** (or **E-2**) self-coupling (less than 5%). After removing the cyanoethyl groups of **V-2** (or **E-2**) by CsOH, the resultant dianion was stabilized by adding $ZnCl_2$ to form complex, which then captured the carbonyl group of triphosgene $Cl_3CO-CO-OCCl_3$ to provide the tertiary precursor **V-3** (or **E-3**). [9, 15*b*]

The title TTP derivatives were synthesized by the similar $P(OMe)_3$ mediate cross-couplings between the tertiary and the primary precursors: **V-3** with **V-1** for **BV-TTP**, **E-3** with **E-1** for **BE-TTP**, **E-3** with **M-1** for **EM-TTP**, and **V-3** with **E-1** for **EV-TTP**, respectively. The feed ratio of the primary precursor : tertiary precursor was taken to be 1.5:1. The solubility of these 12-S-atom TTP derivatives in various solvents is extremely low. Fortunately, they can be considerably dissolved into CS_2 by long-term extracting in an improved Soxhlet's extractor and thus we obtained satisfying crystals for X-ray structure determination. The 8-S-atom TTF derivatives BE-TTF and BV-TTF (bis(vinylthio)-TTF) were also obtained with low yield as by-products in synthesizing **BE-TTP** and **BV-TTP**, respectively. Two structures of **BV-TTP** have been isolated as triclinic $P\bar{1}$ (***t*-BV-TTP**) and monoclinic $P2_1$ (***m*-BV-TTP**) separately (see experimental section).

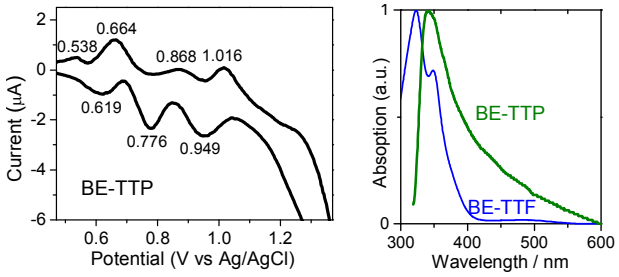

(a) (b)

Fig.1 (a) Cyclic voltammogram of **BE-TTP**; (b) UV-vis absorption spectra of **BE-TTP** and BE-TTF in toluene.

Table 1 Redox potentials (E/V vs Ag/AgCl) and ^{1}H NMR chemical shift δ (see ESI for spectra)

	E_1	E_2	ΔE_{12}	E_3	δ (ppm)	
BE-TTF	0.66	0.86	0.20			3.29 ($-CH_2CH_2-$)
BE-TTP	0.58	0.72	0.14	0.91		3.61 ($-CH_2CH_2-$)
EM-TTP	0.63	0.76	0.13	0.92	5.25($-CH_2-$)	3.60 ($-CH_2CH_2-$)
EV-TTP	0.67	0.80	0.13	0.94	6.84(-CHCH-)	3.60($-CH_2CH_2-$)
BV-TTP	0.68	0.81	0.13	1.00	6.85 (-CHCH-)	
BV-TTF	0.82	0.98	0.16		6.55 (-CHCH-)	
TTF					6.31 (-CHCH-)	

As depicted in Fig. 1a, for example, the cyclic voltammogram of the **BE-TTP** exhibits four pairs of redox-pair. The pair at the highest positive potential is irreversible, while the other three are quasi-reversible. The E_1 values (in Table 1) show a sequence:

BE-TTP < BE-TTF; **BV-TTP** < BV-TTF

indicating that the electron donating ability of the 12-S-atom **BE-TTP** and **BV-TTP** is larger than that of 8-S-atom BE-TTF and BV-TTF, respectively.

The ΔE_{12} (= E_2-E_1) was interpreted to be a measure of the on-site Coulomb repulsion for a pair of electrons.[9] The ΔE_{12} values here in Table 1 show a decrease when going from BE-TTF to **BE-TTP**, and from BV-TTF to **BV-TTP**. Considering the fact that the less Coulomb repulsion of the electrons is corresponding to the larger π-dimension of the molecule, thus the smaller ΔE_{12} value of the 12-S-atom TTP derivatives should be the result from their larger π-dimension (see ESI for extended discussion).

The red-shift ($\Delta\lambda_{abs}$ =18 nm) of the UV-vis absorption peak of **BE-TTP** (relative to BE-TTF, Fig. 1b) and the slightly shorter terminal C-C bond length of **BE-TTP** (relative to BE-TTF) also indicate its better π-conjugation (see ESI for details).

Notably, the ^{1}H NMR chemical shifts (see Table 1) show a consistent sequences

BE-TTP, **EV-TTP**, **EM-TTP** > BE-TTF (for -CH_2CH_2-)

BV-TTP, **EV-TTP** > BV-TTF > TTF (for -CHCH-).

This may be also related to the relatively larger π-dimension of the title TTP derivatives.

2.2 Structure

2.2.1 Triclinic *t*-BV-TTP *vs* monoclinic *m*-BV-TTP

As shown in Figs. 2 and 3, the ***t*-BV-TTP** molecule takes a planar conformation with its central $C_{10}S_{12}$ skeleton being basically co-planar, while the $C_{10}S_{12}$ skeleton of the ***m*-BV-TTP** molecule is wavy-shaped but does not deviate from planarity very much. The calculated energy of the optimized wavy ***m*-BV-TTP** molecule is slightly (0.13 eV) lower than that of the planar ***t*-BV-TTP** molecule. This means that the lattice energy of the triclinic ***t*-BV-TTP** should be larger than that of the monoclinic ***m*-BV-TTP** crystal, so that the extra stabilization of ***t*-BV-TTP** crystal in the packing process can compensate the relatively higher molecular energy. The crystal density of ***t*-BV-TTP** is indeed higher than that of ***m*-BV-TTP** (see Table 3). The length of the C=C bonds in the centre of the TTF unit (C_5=C_6 or C_9=C_{10}) are slightly longer than that of other four C=C bonds. The average C-S bond lengths (see Table 3) are shorter than that of the single C-S bond, indicating the high degree of π-conjugation of these molecules.

Both crystals are characterized by uniform one-dimensional (1-D) columnar structure. In a column, the intermolecular spacing in ***t*-BV-TTP** (3.58 Å) is smaller than that in ***m*-BV-TTP** (3.99 Å), and the offset along the long molecular axis of ***t*-BV-TTP** (5.0 Å) is shorter than that of ***m*-BV-TTP** (8.2 Å), showing the larger π-π overlap in ***t*-BV-TTP**. The electronic transfer integral (t), calculated by equation (4), of a face-to-face pair in ***t*-BV-TTP** (t_1 = 0.144 eV) is also larger than that in ***m*-BV-TTP** (t_1 = 0.129 eV), indicating the stronger 1-D π-π interactions.

The molecular columns are connected *via* S...S side-by-side links (see Figs. 2b-5b for the S...S distances) to build a kind of two-dimensional (2-D) molecular slab. When viewing along the long molecular axis (Figs. 2b-5b), this kind of 2-D slab can fit into a 2-D rhombic lattice, which has been called β-type 2-D slab.[17,2c] The face-to-face intra-column 1-D interactions (indicated by t_1, t_2 values) are several times larger than the side-by-side 2nd-dimensional (2nd-D) inter-column interactions (t_3, t_4).

In ***t*-BV-TTP**, all molecules in the same molecular slab or in different slabs are parallel arranged to form a β-based all-parallel structure (Fig. 2c). In ***m*-BV-TTP**, however, molecules in two neighbouring slabs are in two directions and it can be described as β-based half-parallel or herring-bone packing (Fig. 3c). Though the 1-D face-to-face interactions of ***t*-BV-TTP** are stronger than those of ***m*-BV-TTP**, the third-dimensional (3rd-D) interactions of ***t*-BV-TTP**, characterized by the head-to-tail connections and the t_5, t_6 values, are weaker than those of ***m*-BV-TTP.** This can explain the very thin slice shape of the ***t*-BV-TTP** crystal.

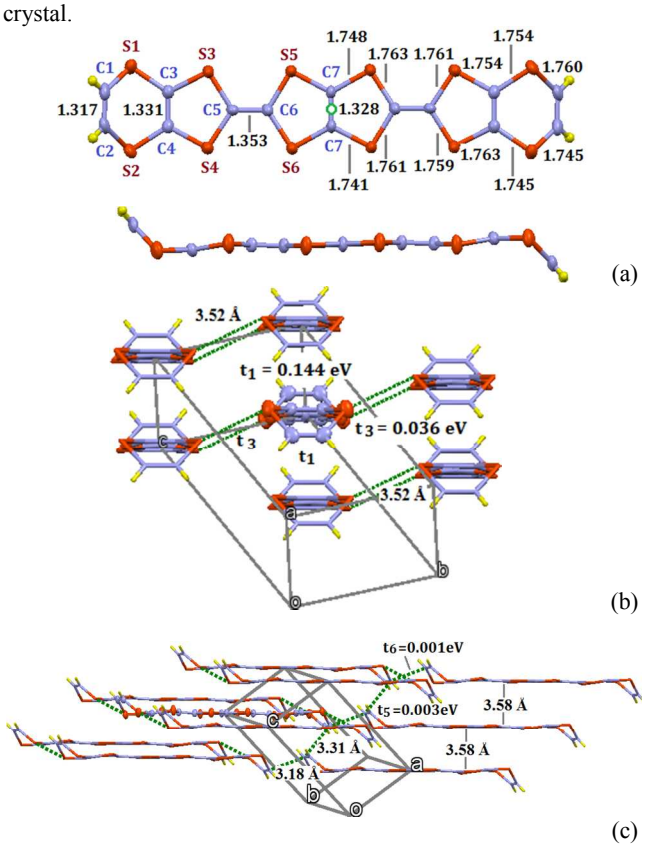

Fig. 2 Structure of the triclinic ***t*-BV-TTP**. (a) Half the molecule is in the asymmetric unit. Mean σ (C-C) = 0.005 and σ (C-S) = 0.003 Å. (b) View along the long molecular axis showing the 1-D columnar structure and β-type 2-D slab. (c) The all-parallel 3-D structure.

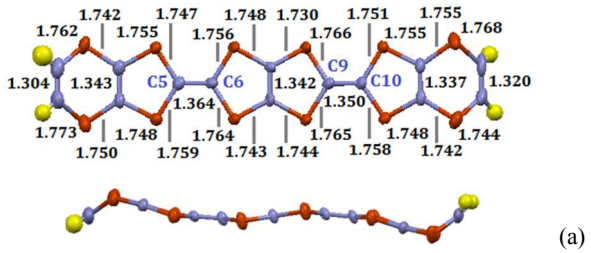

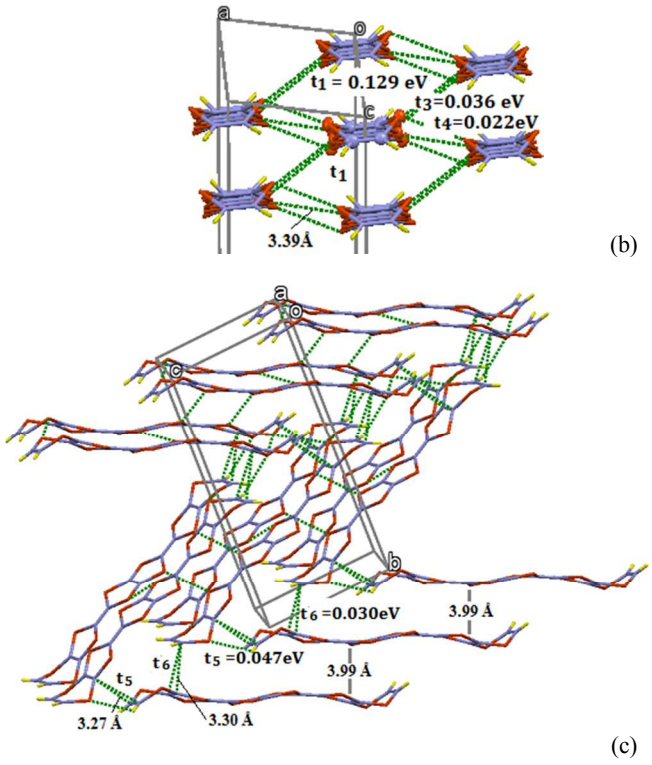

Fig. 3 Structure of ***m*-BV-TTP**. (a) One wavy-shaped molecule is in the asymmetric unit, mean σ (C-C)= 0.008 and σ (C-S) = 0.005 Å. (b) View along the long molecular axis. (c) The herring-bone 3-D structure.

2.2.2 EM-TTP and BE-TTP

As shown in Figs. 4a and 5a, **EM-TTP** and **BE-TTP** molecules adopt a "swimmer-shaped" conformation, with its head and tail being above and below the planar C_6S_8 body. The terminal C-C bond lengths are slightly shorter than typical single C-C bond.

EM-TTP takes a β-based all-parallel packing style, which is similar to ***t*-BV-TTP**. The 1-D column of **EM-TTP** shows a slight dimer structure. It has the shortest spacing (d = 3.47 Å) and largest t_1 value (0.225 eV) in the dimer. Another kind of π-π interactions (d = 3.54 Å, t_2 = 0.184 eV) is also stronger than those in other three crystals. **BE-TTP** takes a β-based herring-bone packing mode similar to ***m*-BV-TTP**, with its 1-D π-π interactions (d = 3.55 Å, t_1 = 0.173 eV) being stronger than those of ***m*-BV-TTP**.

The 3rd-D interactions of **EM-TTP,** indicated by the head-to-tail weak hydrogen bonds and small t_5 value, are weak. Thus the shape of the **EM-TTP** crystal is thin slice (see Fig. 8 in ESI). On the other hand, the head-to-tail 3rd-D interactions (t_5 = 0.074 eV) of **BE-TTP** are so remarkable that they are comparable to the side-by-side 2nd-D interactions (t_3 = 0.033 eV).

In short, the all-parallel β-structure (**EM-TTP** and ***t*-BV-TTP**) has strong 1-D face-to-face π-π interactions, while the half-parallel herring-bone β-structure (**BE-TTP** and ***m*-BV-TTP**) has more 3-D characters.

We also calculated the transfer integral (t) of the non-capped 12-S-atom TTP derivatives TTM-TTP and TTC_4-TTP by the same method based on the CCDC data. As shown in Fig. 10 (in ESI), their 2-D interactions are weak. The terminal alkyl groups make the molecules depart from normal face-to-face overlap.

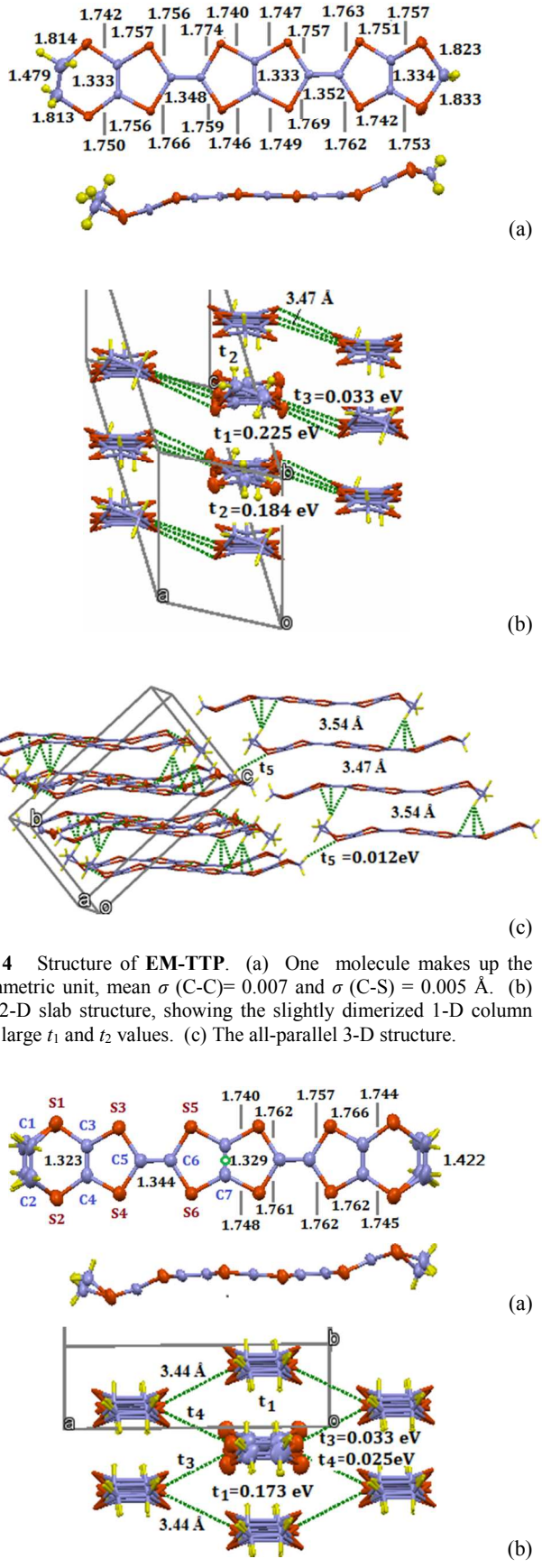

Fig. 4 Structure of **EM-TTP**. (a) One molecule makes up the asymmetric unit, mean σ (C-C)= 0.007 and σ (C-S) = 0.005 Å. (b) The 2-D slab structure, showing the slightly dimerized 1-D column with large t_1 and t_2 values. (c) The all-parallel 3-D structure.

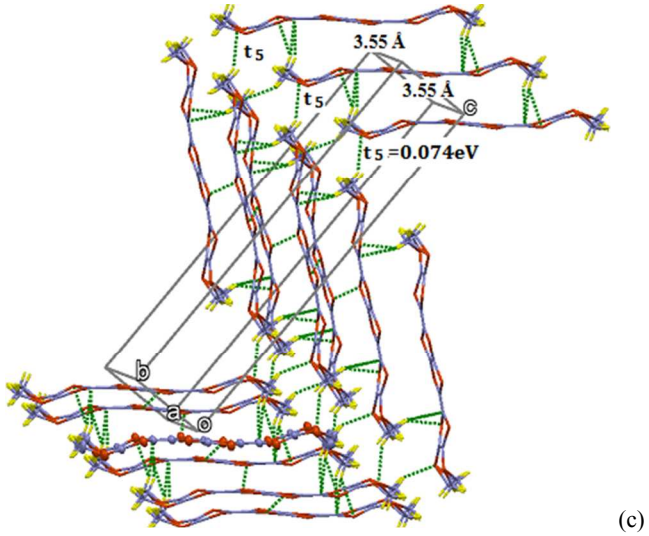

(c)

Fig. 5 Structure of **BE-TTP**. (a) Half of the centro-symmetric molecule is in the asymmetric unit, σ (C-C), σ (C-S) = 0.005, 0.004 Å. The ethylene groups are disordered, while its C-C bond length is from a non-disordered treatment. (b) (c) The molecular packing is similar to ***m*-BV-TTP**, with stronger 1-D and 3rd-D interactions.

2.2.3 EV-TTP

EV-TTP molecules are arranged in trimers (Figs. 6a, 6c). In a trimer, the planar molecule is located at the crystallographic symmetric centre and thus disordered, while two satellite molecules take a boat-like conformation and are π-π overlapped to the central molecule with a spacing being 3.57 Å.

By contrast with the above four β-type structures, the packing of **EV-TTP** can be referred to as the three-by-three κ-type, as an extension of the well known κ-phase featuring perpendicularly arranged dimer or tetrad donors in some BE-TTF salts. The reported κ-pattern are the view along the long axis of the donor, [18-20, 2a-b] however, the κ-pattern shown in Fig. 6c is the view along the short axis of the **EV-TTP** molecule.

In a κ-type 2-D molecular sheet (Fig. 6c), the face-to-face π-π interactions (t_1 = 0.203 eV) are limited within the trimer, not extending to the 1-D interactions. Another kind of interesting head-to-body intermolecular interactions can be observed by viewing the large t_5 (0.178 eV) and t_6 (0.115 eV) values. The CC' distances in the C-H...C' hydrogen bond are 3.42 Å in the t_5 interaction pair and 3.43 Å in the t_6 interaction pair, respectively.

The side-by-side S...S interactions, though not very strong (t_1 = 0.021 eV), run through the crystal at [100] direction (see Fig. 6b). In a word, the face-to-face, head-to-body, and the side-by-side interactions in **EV-TTP** help to build the best 3-D structure in these crystals.

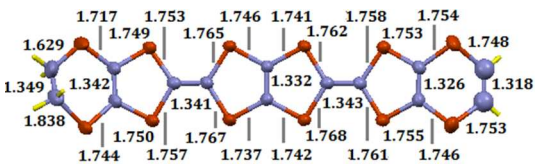

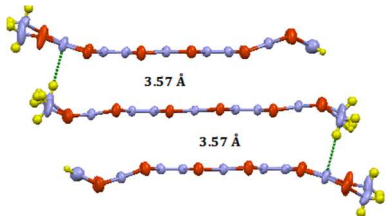

(a)

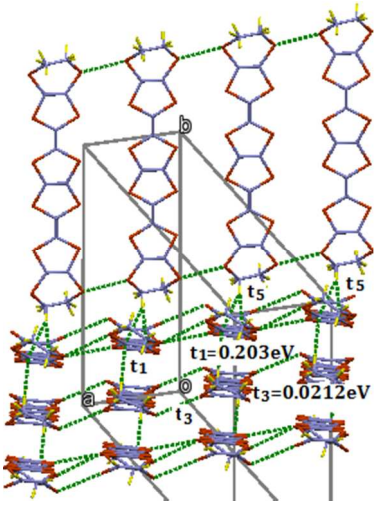

(b)

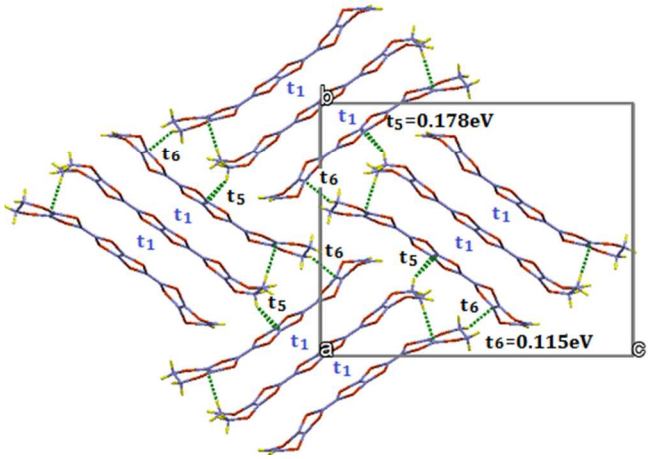

(c)

Fig. 6 Structure of **EV-TTP.** (a) One and a half molecules, which compose the asymmetric unit, being centro-symmetrically inverted to a trimer. The indicated bond lengths, which have the standard deviations of σ (C-C)= 0.004 and σ (C-S) = 0.003 Å, are of the boat-like molecule. (b) The view along the long molecular axis. (c) The short-axis view of the structure showing the κ-type 2-D sheet.

2.3 Charge transport properties

2.3.1 Electrical conductivities

The electrical conductivities of the long-plate crystal of **BE-TTP**, long thin-slice crystal of **EM-TTP,** long-bar crystals of ***m*-BV-TTP** and **EV-TTP** were measured by the two-probe method at room temperature (These crystals are shown in Fig. 9 in ESI). For example (see Fig. 11 in ESI), two gold wires, 0.03 mm in diameter and 1.2 mm apart from each other, were run

perpendicularly across a long-bar-shaped **EV-TTP** crystal with a dimension of 1.8 × 0.08 × 0.04 mm and fixed in place using gold paste. Two avometers (VC9808 and MF500B) were used for the conductivity measurements to check the data. The measurements were carried out on several samples of every kind of crystal and the results were well repeatable in a period of one month. The as-measured conductivities (listed in Table 2) were along the long axis of the crystals, which were indexed by X-ray diffraction to be the [010] direction (the face-to-face columnar direction) for **BE-TTP**, the [100] direction (the side-by-side direction) for ***m*-BV-TTP**, **EM-TTP**, and **EV-TTP** (see Fig. 9 in ESI for the indexing method).

For the herring-bone β-structure, the 1-D and 3rd-D interactions of **BE-TTP** (t_1, t_5 = 0.173, 0.074 eV) are stronger than that of ***m*-BV-TTP** (t_1, t_5 = 0.129, 0.047 eV), respectively. This can partly explain why the conductivity of **BE-TTP** is two orders of magnitude larger than that of ***m*-BV-TTP**. This difference of conductivity can be also attributed to anisotropy. For **BE-TTP**, the [010] is the direction of the face-to-face 1-D column, which is the most conductive direction. However, the [100] of ***m*-BV-TTP** is the direction of the side-by-side direction, not the most conductive direction. One may argue why the column direction of ***m*-BV-TTP** is not the actual dominant direction [100] of crystal growth. This is because of the relatively large side-by-side interactions of ***m*-BV-TTP** (t_3/t_1= 0.28) in comparison to the case of **BE-TTP** (t_3/t_1= 0.19), and of the fact that one molecule has four side-by-side neighbours while two face-to-face neighbours.

EM-TTP crystal has an all-parallel β-structure and exhibits a high conductivity of 7×10^{-3} Ω^{-1}cm^{-1} in [100] direction, which is the side-by-side direction but not the most conductive [010] columnar direction. At the [010] direction, however, the small size (~0.1 mm) of the crystal make the reliable measurement very difficult. **EV-TTP** crystal exhibits a conductivity of 3×10^{-3} Ω^{-1}cm^{-1} in [100] direction.

2.3.2 Hole mobility calculations

The sulfur-rich donor compounds belong to p-type organic semi-conductors and their hole transport can be described by the hopping of a electron between a molecule and a neighbouring cation (hole) shown below

$$M \cdots M^{+} \rightarrow M^{+} \cdots M \quad (1)$$

Base on the Marcus electron-transfer theory, the charge-transfer rate, k, can be expressed by [21, 22]

$$k = \frac{1}{\hbar}\left(\frac{\pi}{\lambda k_B T}\right)^{1/2} t^2 \exp(-\frac{\lambda}{4k_B T}) \quad (2)$$

The most important term in the above expression is the reorganization energy λ, which can be regarded as the energy barrier (the smaller, the better) for charge transport and can be expressed by [23]

$$\lambda = \lambda_1 + \lambda_2 = (E_+^0 - E_0^0) + (E_0^+ - E_+^+) \quad (3)$$

where the λ_1 measures the energy difference between the stable neutral molecule and the molecule with the cation geometry, λ_2 measures the energy difference between the cation at its stable state and the cation at the Franck-Conton state.

The second important term in equation (2) is the electronic transfer integral t, which denotes the electronic coupling (the larger, the better) between a charge-transfer pair and can be calculated by [24]

$$t = \frac{1}{2}(E_{\text{HOMO}} - E_{\text{HOMO-1}}) \quad (4)$$

Where E_{HOMO} and $E_{\text{HOMO-1}}$ are the energy levels of the HOMO and HOMO-1orbitals of a two-molecule-pair. All the t values indicated in Fig. 2-6 were calculated in this way.

If there exists a dominant direction for charge transport, such as the π-π columnar structures of ***t*-BV-TTP**, ***m*-BV-TTP**, **BE-TTP**, and **EM-TTP**, only one matrix element of t, corresponding to a face-to-face pair, needs considering. We took the two-molecule-pair from the X-ray crystal structure without geometric optimization.

By introducing the known relation between the hopping rate k and the diffusion coefficient D

$$D = \frac{1}{2}d^2 k \quad (5)$$

where the d is the π-π spacing of the 1-D molecular column, and by introducing the well-known Einstein relation

$$\mu = \frac{e}{k_B T} D \quad (6)$$

the hole mobilities, μ, of the title TTP derivatives have been calculated (at 300 K) and listed in Table 2.

Table 2 Measured conductivities and calculated charge transport properties

	σ (Ω^{-1}cm^{-1})	λ (eV)			t (eV)	μ (cm^{2}V^{-1}s^{-1})		
		free	cage-1	cage-2		free	cage-1	cage-2
***t*-BV-TTP**		0.299	0.203	0.106.	0.144	0.88	2.69	9.98
***m*-BV-TTP**	2×10^{-5}	0.299	0.236	0.123	0.129	0.87	1.81	7.41
BE-TTP	1×10^{-3}	0.320	0.210	0.170	0.171	1.19	4.26	9.44
EM-TTP	7×10^{-3}	0.311	0.201	0.143	0.209	1.54	5.53	11.5
EV-TTP	3×10^{-3}	0.316						
DT-TTF		0.254	0.257	0.150	0.100	0.73	0.71	2.59

The λ calculation is usually based on the optimized geometries of a free molecule and a free cation. The as-calculated λ and μ values are listed in the "free" columns in Table 2.

Having noticed the difference between a molecule/cation (the host) in freedom and the host in crystal, Bromley introduced the embedded-approach (more exactly the cage-approach), by which the host being optimized is surrounded by several guest molecules with fixed X-ray structure (freezing coordinates). [25] The λ value of DT-TTF (dithiophene-TTF, see Scheme 1) was greatly reduced from 0.24 eV by the free-approach to 0.042 eV by the cage-approach.[25] However, in the course of geometric optimization, Bromley did not cage the cation's charge and left 0.28 positive charge on it, which may make the λ value too low.

In our treatment (cage-1 approach), the charge of cation was constrained to +1 (mono-cation) by using the "oniom" order of the Gaussian-03 programs combined with the (0 1 1 2 0 1) charge-multiplicity code.[26] The λ and μ values of DT-TTF (in cage-1 column in Table 2) are essentially the same as that of the free-approach. However, the μ values of our four β-structural

crystals (***t*-BV-TTP**, ***m*-BV-TTP**, **BE-TTP**, and **EM-TTP**) are more than two times that of the free-approach, which can be attributed to a one-third reduction of the λ values (approximately from 0.3 to 0.2 eV). To cage a host, at least two guest molecules are needed (from the above and below of the host in the 1-D column). The λ value is slightly getting smaller and tends to converge to $\lambda_{min,}$ when the number of guests is increasing. In practice, as schematically shown in Figs. 2b, 3b, and 5b, we took six guests (drawn by the capped sticks) to cage one central host (drawn by the ellipsoid).

One of the most intriguing structural features of TTF derivatives is the so-called fractional charge state, e.g., the well-known half-charged state, in their charge-transfer radical-cation salts.[2] The stoichiometry of $(BE\text{-}TTP)_2I_3$, for example, implies that the formally half-charged state may be interpreted as two **BE-TTP** molecules sharing one charge, $[(BE\text{-}TTP)_2]^+$, and this dimeric-ion may play the role of charge carrier in the hopping process described below

$$(MM)^{\cdots}(MM)^{+} \rightarrow (MM)^{+\cdots}(MM) \qquad (7)$$

With these ideas in mind, we then introduce the cage-2 approach for our TTP derivatives. The dimeric-molecule MM or dimeric-ion $(MM)^+$ in crystal is taken as the central host (dimer-host) for geometric optimization, which is caged by eight guest molecules in crystal with fixed coordinates (schematically shown in Fig. 4b). The detailed calculating methods, including the "oniom" order and the charge-multiplicity code in the input file, are the same as the cage-1 approach and the results are listed in cage-2 column in Table 2.

All the λ values of the cage-2 approach are significantly smaller than those of the cage-1 approach, indicating the much lower energy barrier for the dimeric-ion hopping expressed by equation (7). Consequently, the μ values by cage-2 approach are several times larger than those by cage-1 approach and one order of magnitude larger than those by the free-approach. Noticeably, the as-calculated (cage-2) μ value (2.59 cm^2/Vs) of DT-TTF is comparable to the measured one (μ = 3.6 $cm^2\ V^{-1}s^{-1}$),[27] giving an experimental test to the cage-2 approach.

As listed in Table 2, the calculated hole mobilities (μ) of the four β-structural crystals (***t*-BV-TTP**, ***m*-BV-TTP**, **BE-TTP**, and **EM-TTP**) are invariably larger than that of the OFETs crystal DT-TTF. This can be attributed to, among other factors, their large electronic transfer integral *t*. Note that the calculated mobility shows the sequence of

EM-TTF > BE-TTF > *m*-BV-TTP,

which is in consistent with the sequence of the measured conductivities. Based on its larger calculated μ value, ***t*-BV-TTP** is expected to have higher conductivity than ***m*-BV-TTP**, but unfortunately the crystal is too small and thin to make the measurement.

3 Conclusions

This work made a detailed synthesis-structure-property investigations on several full-capped 12-S-atom TTP derivatives. Several conclusions can be drawn:

(1) In the viewpoint of the molecular properties: The combined data (redox, UV-absorption, X-ray diffraction, and NMR) indicate that the electronic donating ability and the π-conjugation have an increase when the TTF-core in the full-capped 8-S-atom TTF derivative is replaced by the bis-fused TTF core, yielding the title 12-S-atom TTP derivatives.

(2) In the viewpoint of the solid state properties: The title full-capped TTP derivatives are essentially more conductive than the similar non-capped 12-S-atom TTP derivatives, because there are no redundant alkyl chains and therefore the molecules can be more tightly packed in crystal. The conductivities of **EM-TTP** and **EV-TTP** single crystals are comparable to the highest reported conductivities (by the same two-probe method) of the single-component organic conductors. [13]

(3) In the viewpoint of the structure-property correlations: The maximum anisotropic conductivity and mobility of the all-parallel β-structure (**EM-TTP** and ***t*-BV-TTP**) should be higher than those of the half-parallel (herring-bone) β-structure (**BE-TTP** and ***m*-BV-TTP**), because of the larger 1-D face-to-face π-π interactions along the molecular columns of the former. On the other hand, the herring-bone β-structure and κ-structure (**EV-TTP**) have more 3-D characters of intermolecular interactions. Their charge transport properties should be relatively more isotropic.

(4) The host-caged modeling, both the cage-1 and cage-2 approach, in calculating the hole mobility (μ) of TTF and TTP derivatives seems successful. The calculated μ values of our TTP derivatives are larger than that of the well-known OFETs crystal DT-TTF. It deserves to make a further experimental investigation on the OFETs properties of the title TTP derivatives in our near future.

4 Experimental section

4.1 Synthesis and chemical characterization

Trimethyl phosphite $P(OMe)_3$ was distilled under N_2 atmosphere by fractional distillation. CS_2 was dried over Na_2SO_4 and distilled twice prior to use. Solvents were purified by the standard methods. All the reactions were carried out under N_2 atmosphere. Whenever reactant or solvent was added to the reaction system, three turns of pump-nitrogen circling immediately followed. MS and HR-MS data were recorded by Kratos PC Axima CFR plus V2.4.0 mass spectrometry and Thermo Fisher Scientific LTQ FT Ultra mass spectrometry, respectively. NMR spectra were recorded on a Bruker Advance-300 NMR spectrometer, CS_2 was used as the solvent with $CDCl_3$/TMS being the external references for the title compound. Because of the poor solubility, the NMR tubes have to be sealed and heated to 80°C for about one week and some spectra were recorded overnight. IR spectra were recorded on a Thermo Nicolet Avatar 370 FTIR spectrometer. TG-DTA curves were recorded on a Perkin-Elmer Diamond instrument under a dry nitrogen flow, with a heating rate of 10 °C min^{-1}. These curves (Fig. 12 in ESI) show the title compounds are stable at least to 200 °C.

The redox potentials were measured by cyclic voltammetry on a PARSTAT 2273 potentiostat in benzonitrile-CS_2 (1:1, v/v) solutions (0.10 mM for BE-TTF or BV-TTF, 0.01 mM for the 12-S-atom TTP derivatives) containing 0.1 M n-Bu_4NClO_4 as a supporting electrolyte at a scan rate 50 mVs^{-1} under N_2 atmosphere at 20 °C. The Pt wires were used as working and

counter electrodes, Ag/AgCl as reference electrode for all the compounds listed in Table 1.

2,5-Bis(4,5-vinylenedithio-1,3-dithiol-2-ylidene)-1,3,4,6-tetrathiapentalene (BV-TTP)

To a three-neck flask, 0.089 g of (0.40 mmol) 4,5-vinylenedithio-1,3-dithiole-2-thione (**V-1**) was added and dissolved in 10 mL toluene by heating. When the hot yellow solution was cooling to 50°C, 0.101 g (0.26 mmol) of 2-(4,5-vinylenedithio-1,3-dithiol-2-ylidene)-5-one-1,3,4,6-tetrathiapentalene (**V-3)** and 7 mL freshly distilled $P(OMe)_3$ was added. In the course of heating and temperature rising (to 110°C), the mixture became clear orange solution, then precipitate appeared at 95°C. It was kept refluxing at 110°C for 20 h and allowed to stay in a refrigerator (-10°C) overnight. MeOH (5 mL) was added and the product was filtered, washed by MeOH and dried, to give 0.096 g brown solid, which was then transferred into a Soxhlet's extractor and extracted by CS_2 in the dark and in the absence of oxygen (see Fig.13 in ESI).

The first crop of the extracting solution (the crop of 4 days' extracting) was treated by column chromatography (silica gel). The column was initially eluted by hexane to remove trace of S_8 and other impurities and then eluted by CS_2. The first useful fraction proved to be BV-TTF, the resultant of **V-1** self-coupling. The CS_2 solution of the second fraction, after slowly evaporating out of the CS_2 solvent, gave 14 mg of thin-slice orange crystals, which proved to be the triclinic ***t*-BV-TTP** by X-ray structure determination (Fig. 2 and Table 3). MS (MALDI-TOF): *m*/*z* 556.0 (M^+); HR-MS (MALDI): calculated for $C_{14}H_4S_{12}$: 555.6956, found 555.6955. IR (KBr, ν/cm^{-1}): 3025w, 2972w, 2922w, 1575w, 1505w, 962m, 901s, 800s, 762s, 685s, 675s, 597m, 494w, 408s (see ESI for the spectrum).

The second crop of the extracting solution (the crop of about one month's of extracting after the first crop) can be directly used for crystal growth by solvent evaporation and 25 mg of long-bar shaped orange-red crystals was obtained, which proved by X-ray diffraction to be another polymorph of **BV-TTP**, the monoclinic ***m*-BV-TTP** (Fig. 3 and Table 3). MS (MALDI-TOF): *m*/*z* 556.0 (M^+); HR-MS (MALDI): calculated for $C_{14}H_4S_{12}$: 555.6956, found 555.6954. ^{1}H NMR (300 MHz, CS_2, $CDCl_3$/TMS, ppm): 6.85 (s, 4H, S-CH=CH-S). IR (KBr, ν_{max}/cm^{-1}): 3019w, 2922w, 2851w, 1574w, 1501w, 959m, 906s, 802s, 762s, 690s, 676s, 595m, 496w, 408s (see ESI for the spectrum). The total yield (***t*-BV-TTP** plus ***m*-BV-TTP**) is 30%.

The triclinic ***t*-BV-TTP** and monoclinic ***m*-BV-TTP** can be identified by checking a CH peak of the IR spectra, which is at 2972 cm^{-1} for ***t*-BV-TTP** and 2922 cm^{-1} for ***m*-BV-TTP**.

2,5-Bis(4,5-ethylenedithio-1,3-dithiol-2-ylidene)-1,3,4,6-tetrathiapentalene (BE-TTP)

BE-TTP was synthesized by cross-coupling **E-3** with **E-1** and by the similar method above. The mixture of the first circulating extraction was treated by column chromatography. After seperating the by-product BE-TTF by using CH_2Cl_2 in column chromatography, CS_2 was used to elute **BE-TTP**. The second circulating extraction in the same Soxhlet's extractor then followed to obtain the second crop of orange long-plate **BE-TTP** crystals. The orange-red long-plate crystals crystallized from the eluate of column chromatography (the first crop) were used for X-ray structure determination (Fig. 5 and Table 3). Yield, 25%. MS (MALDI-TOF): *m*/*z* 559.6 (M^+); HR-MS (MALDI): calculated for $C_{14}H_8S_{12}$: 559.7269, found 559.7268. ^{1}H NMR (300 MHz, CS_2, $CDCl_3$/TMS, ppm): 3.61 (s, 8H, S-CH_2CH_2-S). IR (KBr, ν_{max} /cm^{-1}): 2919m, 2849w, 1508w, 1402s, 1284s, 1124m, 961m, 902s, 881m, 828m, 763s, 680w, 624w, 500m, 466m, 442m, 404s (see ESI for the spectra).

2-(4,5-Ethylenedithio-1,3-dithiol-2-ylidene)-5-(4,5-vinylenedithio-1,3-dithiol-2-ylidene)-1,3,4,6-tetrathiapentalene (EV-TTP)

By cross-coupling **V-3** with **E-1** and by the extraction-chromatography-extraction procedures as the above, long-bar shaped red **EV-TTP** crystals were obtained. The crystal for X-ray structure determination was from the second crop of CS_2 extraction (Fig. 6 and Table 3). Yield, 26%. MS (MALDI-TOF): *m*/*z* 557.5 (M^+); HR-MS (MALDI): calculated for $C_{14}H_6S_{12}$: 557.7113, found 557.7117. ^{1}H NMR (300 MHz, CS_2, $CDCl_3$/TMS, ppm): 6.84 (s, 2H, S-CH=CH-S), 3.60 (s, 4H, S-CH_2CH_2-S). IR (KBr, ν_{max}/cm^{-1}): 2920m, 2844w, 1542w, 1507w, 1283m, 1123w, 962s, 901s, 800s, 761s, 673s, 594w, 463m, 444m, 408s. The IR spectrum (see ESI) of **EV-TTP** is similar to the spectral overlap of **BE-TTP** and ***m*-BV-TTP**. Its 1283m and 673s sharp peaks, for example, are corresponding to the character peaks of **BE-TTP** (1284s) and ***m*-BV-TTP** (676s), respectively.

2-(4,5-Ethylenedithio-1,3-dithiol-2-ylidene)-5-(4,5-methylenedithio-1,3-dithiol-2-ylidene)-1,3,4,6-tetrathiapentalene (EM-TTP)

By cross-coupling **E-3** with **M-1** and by the same procedures of synthesizing **BE-TTP**, thin-slice orange-red **EM-TTP** crystals were obtained. The crystal for X-ray structure determination (Fig. 4 and Table 3) was from the CS_2 solution through the silica-gel column (the first crop). Yield, 14%. MS (MALDI-TOF): *m*/*z* 545.5 (M^+); HR-MS (MALDI): calculated for $C_{13}H_6S_{12}$: 545.7113, found 545.7114. ^{1}HNMR (300 MHz, CS_2, $CDCl_3$/TMS, ppm): 5.25 (s, 2H, S-CH_2-S), 3.60 (s, 4H, S-CH_2CH_2-S). IR (KBr, ν_{max} /cm^{-1}): 2917m, 2849w, 1508m, 1407m, 1282m, 1094m, 962s, 904m, 852m, 760s, 701w, 682m, 491m, 444m, 409s (see ESI for the spectrum).

4.2 Calculation and X-ray structure determination

All the quantum chemistry calculations, including the geometric optimization, the electronic transfer integral *t*, and the reorganization energy λ, were carried out within the framework of DFT/b3lyp/6-311g(d) by using Gaussian-03 programs. [26]

X-ray single-crystal diffraction (Mo K_α radiation) were carried out with a Bruker APEX II diffractometer and all structures were solved and refined by using the Bruker SHELXTL programs. All the displacement ellipsoids in all Figures were drawn at 50% probability level. The details can be found in CIF files, which are available from the CCDC with the deposition numbers: 942662 (***t*-BV-TTP**), 942663 (***m*-BV-TTP**), 942664 (**BE-TTP**), 942665 (**EM-TTP**), and 968034 (**EV-TTP**).

Cite this: DOI: 10.1039/c0xx00000x

www.rsc.org/xxxxxx

ARTICLE TYPE

Table 3. Structure data of the title crystals

	***t*-BV-TTP**	***m*-BV-TTP**	**BE-TTP**	**EM-TTP**	**EV-TTP**
Formula	$C_{14}H_4S_{12}$		$C_{14}H_8S_{12}$	$C_{13}H_6S_{12}$	$C_{14}H_6S_{12}$
Formula weight /g mol^{-1}	556.90		560.92	546.90	558.91
Crystal system,	Triclinic	Monoclinic	Monoclinic	Triclinic	Monoclinic
Space group	$P\bar{1}$	$P2_1$	$C2/c$	$P\bar{1}$	$P2_1/c$
Z	1	2	4	2	6
Asymmetric unit	0.5 Mol	1 Mol	0.5 Mol	1 Mol	1.5 Mol
T/K	292	210	294	150	294
a/Å	6.2212(3)	6.4084(4)	11.9501(18)	6.4227(4)	6.45720(10)
b/Å	6.4416(3)	17.7164(12)	5.8237(9)	9.4246(5)	19.2326(2)
c/Å	12.3200(6)	9.0918(6)	29.382(4)	16.9326(9)	24.0962(2)
α/°	96.924(4)	90	90	83.890(3)	90
β/°	103.818(4)	109.547(4)	90.876(2)	81.735(3)	97.4460(10)
γ/°	97.070(4)	90	90	70.108(3)	90
V/Å^3	469.99(4)	972.74(11)	2044.6(5)	951.96(9)	2967.24(6)
D_{calc}/g cm^{-3}	1.968	1.901	1.822	1.908	1.877
$F(000)$	280	560	1136	552	1692
Independent reflections	2210	4572	2183	4200	7151
Reflections with $I > 2\sigma(I)$	1255	2811	1721	3160	4399
Parameters, restraints	126, 0	251, 1	138, 0	250, 0	412, 12
R_{int}	0.0521	0.0700	0.0474	0.0274	0.0483
R [$I > 2\sigma(I)$, all data]	0.0418, 0.0937	0.0386, 0.0786	0.0474, 0.0587	0.0572, 0.0797	0.0377, 0.0717
wR_2 [$I > 2\sigma(I)$, all data]	0.0797, 0.0942	0.0610, 0.0684	0.1134, 0.1185	0.1241, 0.1336	0.0836, 0.0908
S (all)	0.928	0.814	0.821	0.906	0.913
$\Delta\rho_{max}$, $\Delta\rho_{minm}$ /e Å^{-3}	0.34, -0.36	0.38, -0.28	0.49, -0.30	0.91, -0.56	0.59, -0.42
θ_{max}/°	27.9	27.9	27.0	27.5	28.0
Completeness	98.3%	99.0%	96.9%	96.0%	99.7%
Mean C=C /Å	1.332(5)	1.337(8)	1.332(5)	1.340(7)	1.336(4)
Shortest C...C /Å	3.180(5)	3.273(8)			
Mean C-S /Å	1.755(3)	1.753(5)	1.755(4)	1.766(4)	1.754(3)
Shortest S...S /Å	3.523(3)	3.389(5)	3.438(4)	3.466(4)	3.483(3)

Acknowledgements

This work was supported by the National Natural Science Foundation of China (Grant Nos. 20972089, 50673054 and 21472116) and a grant from the State Key Laboratory of Crystal Materials. We thank Professor Dao-ben Zhu for valuable discussions, thank Mr. Hua-wen Wen for assistance in measuring the conductivity.

References

[a] *State Key Laboratory of Crystal Materials, Shandong University, 250100 Jinan, P. R. China. Fax: +86 531 88362782; Tel: +86 531 88363497; E-mail: fangqi@sdu.edu.cn*

[b] *School of Chemistry and Chemical Engineering, Shandong University, 250100 Jinan, P. R. China.*
[c] *School of Information Science and Engineering, Shandong University, Jinan 250100, P R China*

† Electronic supplementary information (ESI) available: Photographs of crystals, infrared and ^{1}H NMR spectra, DTA and TG curves of the title full-capped 12-S-atom TTP derivatives, a photograph of a **EV-TTP** crystal and its gold electrode for conductivity measurement, and an extended discussion about electronic donating and π-conjugation of the title TTP derivatives

1 See for example: (*a*) F. Wudl, G. M. Smith and E. J. Hufnagel, *J. Chem. Soc. D, Chem. Commun*., 1970, 1453-1454; (*b*) J. Ferraris, D. O. Cowan, V. Walatka, Jr. and J. H. Perlstein, *J. Am. Chem. Soc*., 1973, 95, 948-949; (*c*) M. R. Bryce, *J. Mater. Chem*., 1995, 1481-1496.
2 See for example: (*a*) H. Urayama, H. Yamochi, G. Saito, K. Nozawa, T. Sugano, M. Kinoshita, S. Sato, K. Oshima, A. Kawamoto and J. Tanaka, *Chem. Lett*., 1988, 55-58; (*b*) J. M. Williams, A. M. Kini, H. H. Wang, K. D. Carlson, U. Geiser, L. K. Montgomery, G. J. Pyrka, D. M. Watkins, J. M. Kommers, S. J. Boryschuk, A. V. S. Crouch, W. K. Kwok, J. E. Schirber, D. L.Overmyer, D. Jung and M.-H. Whangbo, *Inorg. Chem.,* 1990, 29, 3272-3274; (*c*) K. Murata, M. Tokumoto, H. Anzai, H. Bando, G. Saito, K. Kajimura and T. Ishiguro, *J. Phys. Soc. Jpn*., 1985, 1236-1239; (*d*) S. Yang, F. Pop, C. Melan, A. C. Brooks, L. Martin, P. Horton, P. Auban-Senzier, G. L. J. A. Rikken, N. Avarvari and J. D. Wallis, *CrystEngComm*, 2014, 16, 3906-3916.
3 Y. Misaki, T. Matsui, K. Kawakami, H. Nishikawa, T. Yamabe and M. Shiro, *Chem. Lett.*, 1993, 1337-1340.
4 (*a*) T. Mori, Y. Misaki, H. Fujiwara and T. Yamabe, *Bull. Chem. Soc. Jpn*., 1994, 67, 2685-2689; (*b*) Y. Misaki, H. Fujiwara, T. Yamabe, T. Mori, H. Mori and S. Tanaka, *Chem. Lett*., 1994, 1653-1656; (*c*) A. Deluzet, P. Batail, Y. Misaki, P. Auban-Senzier and E. canadell, *Adv. Mater*., 2000, 12, 436-439; (*d*) S. Perruchas, K. Boubekeur, E. canadell, Y. Misaki, P. Auban-Senzier, C. Pasquier and P. Batail, *J. Am. Chem. Soc*., 2008, 130, 3335-3348.
5 T. Mori, Y. Misaki, T. Yamabe, H. Mori and S. Tanaka, *Chem. Lett*., 1995, 549-550.
6 S. Kimura, S. Hanazato, H. Kurai, T. Mori, Y. Misaki and K. Tanaka, *Tetrahedron Lett*., 2001, 42, 5729-5732.
7 T. Mori, Y. Misaki and T. Yamabe, *Bull. Chem. Soc. Jpn*., 1994, 67, 3187-3190.
8 (*a*) T. Mori, H. Inokuchi, Y. Misaki, H. Nishikawa,T.Yamabe, H. Mori and S. Tanaka, *Chem. Lett*., 1993, 733-736; (*b*) M. Ashizawa, M. Aragaki, T. Mori, Y. Misaki and T. Yamabe, *Chem. Lett*., 1997, 649-650; (*c*) S. Kimura, H. Kurai, T. Mori, H. Mori and S. Tanaka, *Bull. Chem. Soc. Jpn*., 2001, 74, 59-65; (*d*) T. Kawamoto, M. Ashizawa, T. Mori, J.-I. Yamaura, R. Kato, Y. Misaki and K. Tanaka, *Bull. Chem. Soc. Jpn*., 2002, 75, 435-447; (*e*) Y. Bando, T. Matsuzawa, N. Takashita, T. Kawamoto, T. Mori and J.-I. Yamada, *Bull. Chem. Soc. Jpn*., 2005, 78, 1442-1449.
9 (*a*) Y. Misaki, H. Nishikawa, K. Kawakami, S. Koyanagi, T. Yamabe and M. Shiro, *Chem. Lett.*, 1992, 2321-2324. (*b*) The comment from a referee for the previous version this manuscript.
10 (*a*) T. Mori, H. Inokuchi, Y. Misaki, T. Yamabe, H. Mori and S. Tanaka, *Bull. Chem. Soc. Jpn*., 1994, 67, 661-667; (*b*) T. Kawamoto, M. Aragaki, T. Mori, Y. Misaki and T. Yamabe, *J. Mater. Chem*., 1998, 8, 285-288; (*c*) M. Katsuhara, M. Aragaki, S. Kimura, T. Mori, Y. Misaki and K. Tanaka, *J. Mater. Chem*., 2001, 11, 2125-2130; (*d*) M. Katsuhara, S. Kimura, T. Mori, Y. Misaki and K. Tanaka, *Chem. Mater*., 2002, 14, 458-462; (*e*) J. C. Zhong, Y. Misaki, M. Munakata, T. Kuroda-Sowa, M. Maekawa, Y. Suenage and H. Konaka, *Inorg. Chem*., 2001, 40, 7096-7098.
11 Y. Yamashita, S. Tanaka, K. Imaeda, H. Inokuchi and M. Sano, *J. Org. Chem.*, 1992, 57, 5517-5522.
12 S. Kimura, H. Kurai and T. Mori, *Tetrahedron*, 2002, 58, 1119-1124.
13 M. Ashizawa, S. Kimura, T. Mori, Y. Misaki and K. Tanaka, *Synthetic Met*., 2004, 141, 307-313.
14 G. Steimecke, H.-J. Sieler, R. Kirmse and E. Hoyer, *Phosphorus Sulfur*, 1979, 7, 49-55.
15 (*a*) N. Svenstrup, K. M. Rasmussen, T. K. Hansen and J. Becher, *Synthesis*, 1994, 809-812; (*b*) M. Aragaki, T. Mori, Y. Misaki, K. Tanaka and T. Yamabe, *Symthetic Met.*, 1999, 102, 1601-1602.
16 T. Nakamura, T. Nogami and Y. Shirota. *Bull. Chem. Soc. Jpn.* 1987, 60, 3447-3449.
17 T. Mori, *Bull. Chem. Soc. Jpn*., 1998, 71, 2509-2526.
18 T. Mori, H. Mori and S.Tanaka, *Bull. Chem. Soc. Jpn*., 1999, 72, 179-197.
19 A. Kobayashi, R. Kato, H. Kobayashi, S. Moriyama, Y. Nishio, K. Kajita and W. Sasaki, *Chem. Lett*., 1987, 459-462.
20 W. Xu, R. Shen, C.-M. Liu, D. Zhang, D. Zhu, *Synthetic Met*., 2003, 133-134, 349-351,
21 R. A. Marcus, *Rev. Mod. Phys*., 1993, 65, 599-619.
22 K. Sakanoue, M. Motoda, M. Sugimoto and S. Sakaki, *J. Phys. Chem. A*, 1999, 103, 5551-5556.
23 Y. A. Berlin, G. R. Hutchison, P. Rempala, M. A. Ratner and J. Michl, *J. Phys. Chem. A*, 2003, 107, 3970-3980.
24 W.-Q. Deng and W. A. Goddard III, *J. Phys. Chem. B*, 2004, 108, 8614-8621.
25 S. T. Bromley, M. Mas-Torrent, P. Hadley, C. Rovira, *J. Am.Chem. Soc*., 2004, 126, 6544-6545.
26 M. J. Frisch, et al., Gaussian 03 revision B.05, *Gaussian Inc., Pittsburgh PA*, 2003.
27 M. Leufgen, O. Rost, C. Gould, G. Schmidt, J. Geurts, L. W. Molenkamp, N. S. Oxtoby, M. Mas-Torrent, N. Crivillers, J. Veciana and C. Rovira, *Org. Electron*., 2008, 9, 1101.

Graphical and textual abstract

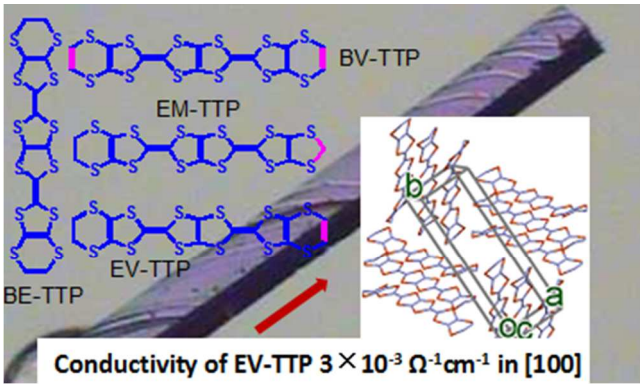

Highly π-conjugated multi-sulfur molecules are tightly packed forming single-component organic crystals with remarkable conductivity.